

# Preparing for Potential Closure of European Airspaces due to Re-entering Space Objects

Enrico Spinielli<sup>✉</sup>, Rainer Koelle<sup>✉</sup> and Quinten Goens<sup>✉</sup>

**Abstract**—The recent decades observed an increasing number of space activities resulting in higher numbers of re-entries at the end of the mission lifespan or orbital decay. The risk of collision between uncontrolled re-entering space debris and aircraft is increasing due to both ever-growing number of airborne flights and of orbiting bodies (and relevant re-entries). National and international authorities need to balance safety and economic impact of adopted measures should a re-entry event be announced, usually on short notice. We employ hourly and daily spatial flight densities calculated from trajectories as recorded by EUROCONTROL’s Network Manager and binned with the Uber H3 geospatial indexing system. Impact risk probabilities are then calculated based on previous theoretical work. This work enhances the model by employing using actual flown flight trajectories as a basis for time-varying flight densities rather than relying on proxies such as the population density or ADS-B/Mode S message counts. These densities combined with a buffered area along the eventual path of re-entry, can provide mid-air impact probabilities to authorities as an aid for deciding on safety measures such as airspace closures and/or re-routings.

## I. INTRODUCTION

The quest for space is a driver for technological development. Key milestones include the first human travel to space and circumnavigating the globe, the first and now many succeeding successful landings on the moon, and regular operations of space stations in the orbit. These developments helped to identify options for the wider use of space, benefits, and its commercialisation. This is showcased by an increasing number of activities aimed to generate value through the exploration of space ranging from scientific understanding and experimentation, sustainable production of goods in a non-gravity environment, services, and recently leisure. The increased number of launches, however, also increased the number of artefacts re-entering the atmosphere.

With forecasts predicting a steadily growing number of flights, see Figure 1, and the modern race to commercialise space, there is a need to re-evaluate the risks of collision and casualties due to uncontrolled debris re-entries. The increasing risk landscape poses challenges in terms of oversight and risk management. There is a growing demand by overseeing authorities for new methodologies and tools to assess which safety measures are the most adequate to minimise potential casualties and economic impact.

The increase in space operations does not exist in a vacuum. The continual growth of air traffic - despite temporal bumps - is evidenced by the surging number of flights in Europe [1] and across the world. On-going development/deployment activities of mega-constellations of satellites in Low Earth Orbit Low

Earth Orbit (LEO), such as already active Starlink and OneWeb or planned ones (e.g. Kuiper, Starshield, Xingwang) will add thousand of orbiting objects with a short operational life. Some of these will inevitably re-enter the Earth’s atmosphere in an uncontrolled manner, c.f. Table I.

Aviation safety risk management is a well-established domain in air transportation. Despite the increasing need for situational awareness of space objects and their re-entry, the classical risk avoidance paradigm revolves around restricting the airspace. While the probability of a strike is low, it can result in catastrophic consequences. The growing number of space operations requires NEW - ADVANCED TOOLS. PREVIOUS WORK DID A,B, and MAYBE C - WE DO SOMETHING ON TOP.

This paper develops a practical and straightforward data-driven pipeline to rapidly assess the risk from uncontrolled re-entry of space debris for the European region. Apart from the general risk assessment of potential re-entries, a soon to occur re-entry of debris from a 1972 failed USSR mission to Venus is analysed.

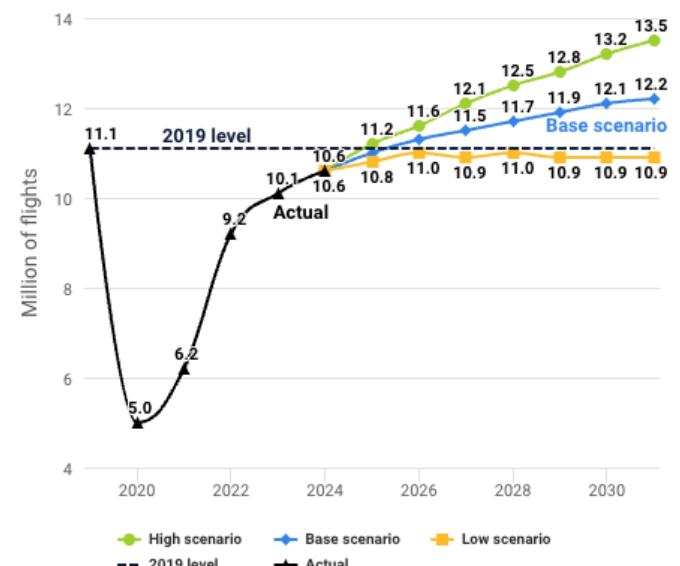


Figure 1: EUROCONTROL 7-year forecast 2025-2031 (Spring 2025).

## II. METHOD

The modelling and tracking of uncontrolled re-entries poses challenges. Actual and historic data is sparse, and the size, shape, and attitude or rotation of re-entering objects increase the level of uncertainty for modelling. Common approaches

Constellation	Country	Launched	Active	Planned	First launch
Starlink	US	4714	3521	4714	2018
Starlink2A	US	3689	3070	6720	2022
Starlink2	US	0	0	30456	-
OneWeb	UK	660	635	716	2019
OneWeb2	UK	0	0	2304	-
Kuiper	US	29	27	3232	2023
StarShield	US	193	126	32	2022
Xingwang	CN	50	10	996	2021
Qianfan	CN	90	28	32	2024
Guangwang	CN	0	0	12992	-
Yinhe	CN	8	7	1000	2020
Hanwha	KR	0	0	2000	-
Lynk	US	10	6	2000	2020
Astra	US	0	0	13620	-
Telesat	CA	0	0	300	-
HVNENET	US	0	0	1440	-
SpinLaunch	US	0	0	1190	-
Globalstar3	DE	0	0	3080	-
Honghu-3	CN	0	0	10000	-
Semaphore	FR	0	0	116640	-
E-Space	US	4	0	337323	2022

Table I: Megaconstellations (planned > 1000) as per filing to the International Telecommunication Union (ITU)

employ a mix of handling the uncertainty of object or debris movement, the associated exposed area, including temporal uncertainty windows.

<!-- is there more to say and provide context -->

In general, the method for estimating the risk to commercial aircraft from re-entering debris objects revolves around estimating the exposure of a single flight and the population of flights to the re-entering object. In that respect, a robust determination of flight density is a key aspect.

We follow the same mathematical approach of [2], [3]. However, this paper augments the approximation of risk exposure. Instead of approximating flight density with population density [2] or aircraft transponder data [3], we use actual flown flight trajectories.

This work focusses on the European region. The hourly flight density estimation is based on flown Instrument Flight Rules (IFR) trajectories as recorded by EUROCONTROL's Network Manager (NM)<sup>1</sup>. To decrease spatial complexity, the data is binned using Uber's H3 geospatial indexing system [4]. The reduction of the spatial complexity enables fast processing. For this work, we employ a H3-cell-resolution of 3. This corresponds to hexagons of an average area 12 393 km<sup>2</sup> and an average edge length of 68.979 km [5] as depicted in Figure 2.

To build an upper threshold for flight exposure, this study uses the busiest week during the International Air Transport Association (IATA) summer ISO week in 2023 and 2024. The flight densities are characterised on an hourly basis for all days in these weeks.

This paper expands the works of [2], [3] and provides a reproducible example for States, Agencies or relevant

<sup>1</sup>NM coordinates Air Traffic Flow and Capacity Management (ATFCM) operations on behalf of EUROCONTROL's 42 Member States and 2 Comprehensive Member States covering almost all European Civil Aviation Conference (ECAC) States, see blue polygon in Figure 2.

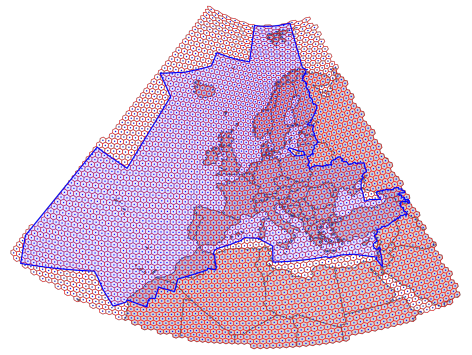


Figure 2: H3 cells (red) at resolution 3 and their centres (blue) covering the bounding box of 43 EUROCONTROL Member States Flight Information Regions (FIRs) (blue shaded polygon).

authorities to build upon.

Next sections will develop the mathematical background for the evaluation of collision expectation of which traffic density is a key component.

Figure 3 shows hourly flight density for the 5th of July 2024. The chart shows the expected outcomes in terms of major traffic flows, and areas of high or low traffic. For example, cells with a density of zero are clearly visible for areas of war or no-fly zones (Ukraine, Libya or Syria). The major traffic flows (North Atlantic, Canaries and East-bound over Türkiye) are clearly highlighted showing densities of more than 10.

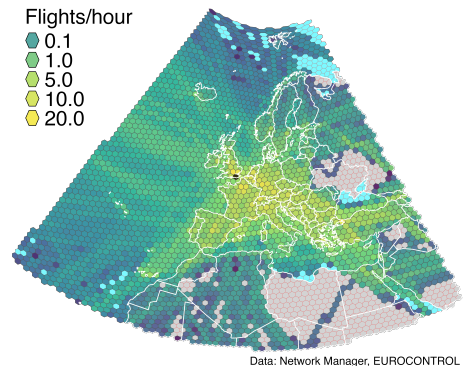


Figure 3: Flight density in the EUROCONTROL Area on the 5th of July 2024, the busiest day of the busiest week in 2024 (H3 cells at resolution 3). The black hexagon in the South of UK marks the densest cell at 24.56 flights/hour, just around the airport of London Heathrow.

#### A. Impact probability for a single flight and single debris

Safety and collision risk awareness is directly linked to the probability of a re-entering space object colliding with a traversing flight. This probability,  $p_k$ , of a debris (point) object  $k$ , impacting an aircraft (point) object over the area,  $a$ , is expressed as:

$$p_k = \varepsilon_k \int_a \rho(\vec{x}) \sigma_k(\vec{x}) da$$

where

- $\rho(\vec{x})$  is the probability density of an aircraft in  $\vec{x}$ ,
- $\sigma(\vec{x})$  is the impact probability density of a debris object  $k$  in the position  $\vec{x}$ , and
- $\varepsilon_k$  is the effective exposed area, i.e., the effective risk area for the  $k^{th}$  debris object impacting the aircraft (see Section II-B later on).

Our approach builds on the discretisation of the geospatial risk area. For this purpose we use a hexagon-based tessellation pattern. Uber's H3 method ensures non-overlapping hexagons (and 5 pentagons), with an equidistant relationship between all neighbours, and enables an efficient indexing of the tessel-cells. Using H3 to discretise the area of interest  $a$  gives

$$p_k = \varepsilon_k \sum_h \rho(h) \sigma_k(h).$$

The impact probability  $p_k(h)$  for each cell  $h$  is determined by the following expression

$$p_k(h) = \varepsilon_k \rho(h) \sigma_k(h). \quad (1)$$

### B. Aircraft effective exposed area

For the actual collision encounter between a re-entering object and an aircraft, we assume the aircraft impact area to be much larger than the debris object area. Thus, the area spanned by the debris object is smaller than the aircraft dimensions. This assumption holds for practically all commercial aircraft within the scope of this study, and we can neglect the debris impact area. Accordingly, we can also simplify the geometry of the aircraft and model it as a rectangular solid with dimensions of wingspan ( $W$ ), length ( $L$ ) and height ( $H$ ).

Regarding the aircraft-debris encounter geometry, this yields to two conceptual considerations:

1. if the aircraft were stationary, the area exposed to the debris impact would be the top face of the rectangular solid, and
2. if the debris were stationary, it would be the front face.

Our focus is on commercial aircraft in flight, and - implicitly - operating at higher altitudes. The en-route portion of a flight is characterised by the aircraft in straight and level flight, moving (mainly) horizontally. At the same time, the falling of the re-entering debris object at regular en-route flight levels will be vertical<sup>2</sup>. This encounter geometry allows to express the effective exposed area,  $\varepsilon_k$ , as

$$\varepsilon_k = \frac{s_a a_h + s_{d_k} a_v}{s_{d_k}} \quad (2)$$

where

- $s_a$  is the average aircraft speed,
- $s_{d_k}$  is the average fall speed of the  $k$ -th debris object,
- $a_T$  area of the aircraft as viewed from the top, and

<sup>2</sup>Even for a ballistic coefficient of 50 lbs/ft<sup>2</sup>, the flight path angle of a re-entering object at 40 000 ft is  $-86.6^\circ$ , which corresponds to nearly vertical descent. Since most debris objects have ballistic coefficients equal to or less than 50 lbs/ft<sup>2</sup>, the vertical descent assumption is a very accurate approximation. [2]

- $a_F$  area of the aircraft as viewed from the front of the aircraft.

This can be further instantiated for specific aircraft types. In the calculations the following is assumed to be true ( $t$  subscript for aircraft type)

- constant debris fall speed  $s_{d_k} = 145$  mph =  $S$  (we adopt this value from pag 7-8 in [2])
- constant aircraft speed,  $s_a = C_t$ , equal to its cruise speed, under the simplification that the majority of the flight time spent cruising,
- aircraft area as viewed from the top,  $a_T = W_t \times L_t = A_t$ , where  $W_t$  is the wingspan, and  $L_t$  the length for the specific aircraft type  $t$
- aircraft area as viewed from the front,  $a_F = W_t \times H_t = F_t$ , where  $W_t$  is the wingspan, and  $H_t$  the height for the specific aircraft type  $t$

The effective exposed area now only depends on the aircraft type  $t$  (i.e., its dimensions and cruise speed) and can be rewritten as:

$$\varepsilon_t = \frac{C_t F_t + S A_t}{S} \quad (3)$$

These aircraft properties are well-known. While there does not exist a single openly available date base for these aircraft parameters, we collected the information from a series of sources and integrated them into a lookup dataset. The values  $W_t$ ,  $H_t$ ,  $L_t$  and  $C_t$  have been retrieved from [6]–[8]; we used  $\varepsilon_t = 1000 \text{ m}^2$  missing entries.

The impact probability for cell  $h$  under consideration of a specific aircraft of type  $t$  becomes:

$$p_{t,k}(h) = \varepsilon_t \rho_t(h) \sigma_k(h) \quad (4)$$

### C. Impact probability density for debris of inclination $i$

Debris that re-enter the Earth's atmosphere via drag-induced decay will fly circular orbits prior to re-entry even if initially on elliptical ones.<sup>3</sup>

The angular position,  $\theta = \omega + \nu$ , of the re-entry point from the ascending node, see Section VI, is uniformly distributed for uncontrolled re-entries,  $\sigma(\theta) = 1/(2\pi)$ . This is due to uncertainties in atmospheric drag (among other things solar activity can expand the atmosphere) and the gravitational effects of the Equatorial bulge. Hence we assume that the impact longitude,  $\lambda$ , is uniformly distributed.

The impact probability density,  $\sigma(\varphi, i)$ , at latitude  $\varphi$  of a re-entering object whose orbit has inclination  $i$  (see Figure 9) is given by (Equation 15 in [2]):

$$\sigma(\varphi, i) = \frac{1}{2\pi^2 R^2 \sqrt{(\sin^2(i) - \sin^2(\varphi))}} \quad (5)$$

<sup>3</sup>In fact drag at perigee will lower apogee and similarly drag at apogee will lower perigee. But because drag at perigee is higher due to denser atmosphere (the perigee is closest to Earth), the apogee will decrease faster than perigee and the orbit will then tend to become a circular one, see figure about apogee/perigee tracking in [9] for empirical evidence.

where  $R$  is the distance from the centre of the Earth of the object potentially being impacted by the debris.

So for example if a building is located at latitude 30 degrees and has an area of  $1000 \text{ m}^2$  and a piece of debris re-enters the Earth's atmosphere from an orbit having an inclination of 45 degrees, the impact probability is given by

$$P = \Delta A \times \sigma(\varphi, i) = 1000 \times \sigma\left(\frac{\pi}{6}, \frac{\pi}{4}\right) \\ = 1000 \times 2.490756 \times 10^{-15} = 2.490756 \times 10^{-12}$$

where we used the equatorial value of 6378 km, for the Earth's radius,  $R$ , as the distance of the building from the centre of the planet.

The impact probability density  $\sigma(\varphi, i)$  for an inclination  $i$  of  $51.7^\circ$  is plotted in Figure 4 and takes a characteristic U shape with zero values for latitudes beyond  $i$ . This density has been derived by simulating a full circular orbit at 550 km height with 10000 positions and calculating the relevant longitudes and latitudes at half degree resolution.

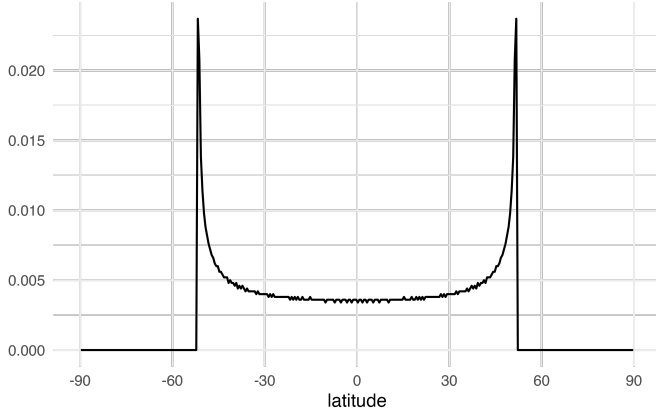


Figure 4: Impact probability density  $\sigma(\varphi, i = 51.7)$  for debris of inclination  $i$  and altitude 550 km.

#### D. Impact probability density for debris

If we consider historical uncontrolled debris re-entry data, we can numerically derive the debris impact probability as a weighting function by summing up and averaging all single densities:

$$\sigma(\varphi) = \sum_k \sigma(\varphi, i_k)$$

From [10] we extracted 1968 debris re-entries during 25 calendar years from 1st Jan 2000 till 31st Dec 2024. The result of combining all the U-shaped densities can be seen in Figure 5.

Spatially projecting  $\sigma(\lambda, \varphi)$  on the H3 cells in the NM area we obtain the weightings per cell (per hour  $H$ ),  $W_H(h)$ , as in Figure 6.

Then Equation 4 becomes

$$p_t(h) = \varepsilon_t \rho_t(h) \sigma(h). \quad (6)$$

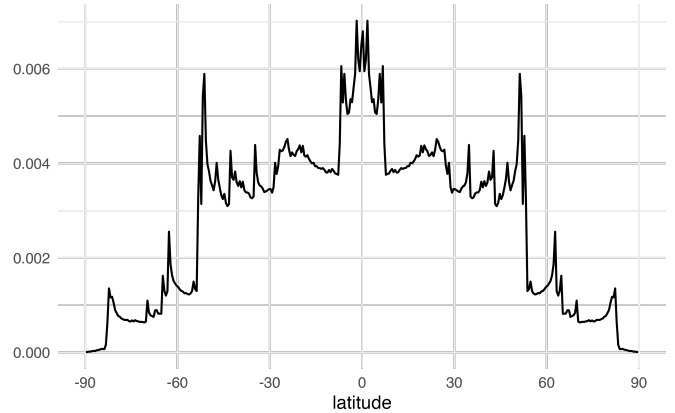


Figure 5: Weighting function derived from 25 years of re-entries as an empirical approximation of  $\sigma(\varphi)$ .

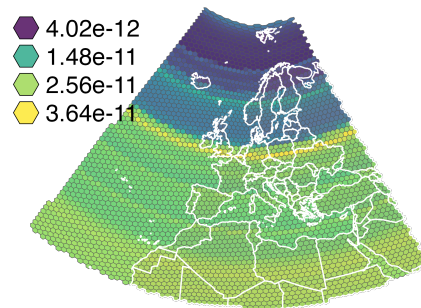


Figure 6: Hourly weightings for H3 cells,  $W_H(h)$ , in NM area.

#### E. Hourly impact probability per H3 cell

When combining the hourly ( $H$ ) aircraft density (per aircraft type) with the relevant weightings per  $h$  cell,  $W_H(h)$ , we can numerically compute the hourly impact probability for each hexagonal cell as:

$$E_{h,H} = \sum_t W_H(h) \cdot \rho_{t,H}(h) \cdot \varepsilon_t$$

where

- $E_{h,H}$  is the collision expectation in the hexagon  $h$  at hour  $H$ ,
- $W(h)$  is the median value of the weighting function over the area of hexagon  $h$ ,
- $\rho_{t,H}(h)$  is the traffic density for the International Civil Aviation Organization (ICAO) aircraft type  $t$  in cell  $h$  at hour  $H$ , and
- $\varepsilon_t$  is effective exposed area for aircraft of type  $t$ .

Figure 7 depicts the determined hourly collision expectation. As identified in Figure 3 areas of higher traffic density observe a higher collision expectation.

### III. USE CASE: KOSMOS 482 DESCENT CRAFT RE-ENTRY

In few days (at the time of writing of this paper) at 23:06 May 10, 2025 ( $\pm 1.8$  days), the KOSMOS 482 Descent Craft should re-enter the Earth's atmosphere [9]. Supposedly the

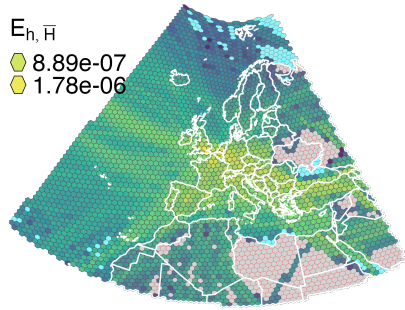


Figure 7: Averaged hourly collision expectation on 2024-07-05.

lander module from a 1972 failed USSR Venera mission [11], it is reported to weigh about 480 kg and to have a diameter of approximately 1 m. Being built to survive Venus's atmosphere which is much denser and hotter than Earth's one (surface pressure 93 times that of Earth and temperatures reaching 467°C (872°F)), it could re-enter Earth intact and not break into smaller fragments some of which could burn up.

Knowing that the debris inclination is 51.7°, see Figure 4, we can derive the maximum collision expectation using data for the busiest day in the busiest 2024 week as a proxy for the traffic density on the day of re-entry. The densest cell, 83194afffffff (area 11 131 585 027 m<sup>2</sup>), at 24.56 flights/hour has centroid latitude of 50.943 69° so within the latitude range of [−51.7°, 51.7°]. Using an average value for effective exposed area of 1000 m<sup>2</sup>, we can quickly calculate the collision expectation as

$$E = w_h \cdot \sigma_h \cdot \bar{\varepsilon} / \text{area}_h \\ = 10^{-6} \cdot 24.56 \cdot 1000 / 11131585027 = 2.2 \cdot 10^{-12}$$

The risk is very low.

Eventually once the re-entry track is known, the H3 cells around 35 km on each side can be identified to retrieve the values of collision expectancy. It can then be decided whether it is advisable to close the airspace and re-route traffic around the area affected.

#### IV. DATA AND CODE FOR REPRODUCIBILITY

We have calculated collision and casualty risk probabilities for the two busiest weeks in 2023 and 2024. The relevant dataset represents a data cube as logically depicted in Figure 8 is available in the companion GitHub repository of the paper at [https://github.com/euctrl-pru/flight\\_density\\_space\\_debris](https://github.com/euctrl-pru/flight_density_space_debris). We have also developed a companion R package aviodebris to heavy-lift the various data processing steps to produce the results in the paper; it is available at <https://github.com/euctrl-pru/aviodebris>.

#### V. CONCLUSION AND FUTURE WORK

Space objects and debris re-entry is an increasing risk to aviation and the general public. The higher pace of commercial space operations will see an increase of launches and subsequent re-entries. Dependent on the mission, objects

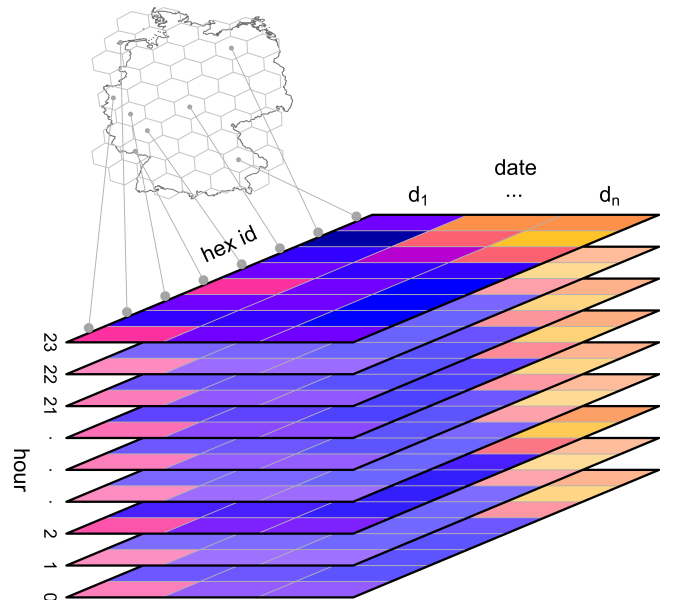


Figure 8: Data cube of hourly flight densities data over H3 hexes (in Germany as an example) for multiple dates,  $d_1 \dots d_n$ .

re-entering the atmosphere can take on different forms, shapes, and sizes. On top, a higher number of these entries may be uncontrolled. With the continual growth of air traffic, there is a need to enhance aviation safety risk awareness and respond in a more tailored fashion to accommodate the associated uncertainties, reduce the impact on aviation, and limit the risk to the travelling public.

This paper expands on previous work. With a focus on Europe, we establish an upper bound for the traffic density based on actual flights.

... SOME MORE STUFF DONE IN THE PAPER ...

The findings are applied to a use-case: the imminent re-entry of the lander module of an earlier Venus mission. The maximum collision expectation for the busiest day in 2024 is determined.

The approach presented in this paper builds on previous research. Our approach utilises H3-tessellation to reduce the spatial complexity. This cell indexing approach reduces the computation significantly.

WHAT ARE THINGS THAT ARE "WEAKNESSES" = STUFF

Future work will address the shortcomings.

We show how National and/or International authorities could prepare for the more and more likely and frequent occurrence of uncontrolled re-entry of space objects that could pose a safety concern on civilian aviation. The techniques we implemented on realistic data and sound algorithms can contribute to the bag of tools in the hands of technical and political entities aiming at guaranteeing the utmost safety and minimal economic disruption to civil aviation in Europe.

As part of this research and to inform the decision-makers it is planned to explore the impact of megaconstellations and

flight growth forecast and what would happen in the mid- to long-term in various scenarios of uncontrolled re-entries and the risk for European airspace.

## VI. APPENDIX: ORBITAL ELEMENTS

We refer to Figure 9 to describe the orbital parameters of interest for the current work.

The angular position,  $\theta$ , of the re-entry point from the ascending node in the orbit plane is  $\theta = \omega + \nu$ . It is related to the latitude,  $\varphi$ , via the Cartesian coordinate  $k$ ,  $k = R \sin(\varphi) = R \sin(\theta) \sin(i)$ , or

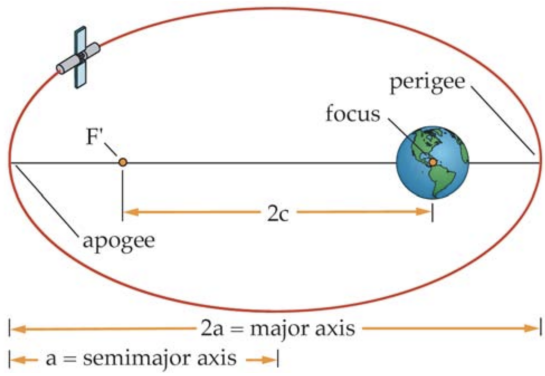
$$\sin(\varphi) = \sin(\theta) \sin(i) \quad (7)$$

Mass of Earth,  $M_{\oplus} = 5.9722 \times 10^{24}$  kg.

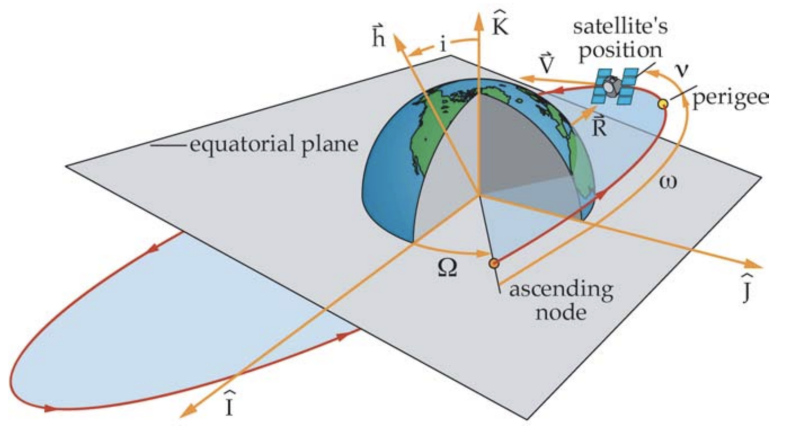
These are used to derive numerically compute the weighting function, Figure 4: for debris with inclination  $i$  we simulate an orbit of  $N$ , i.e. 10001, positions and calculate the corresponding Cartesian position and the equivalent longitude and latitude.

## REFERENCES

- [1] Statfor, “EUROCONTROL Forecast Update 2025-2031 - Spring Update | EUROCONTROL,” 28-Feb-2025. [Online]. Available: <https://www.eurocontrol.int/publication/eurocontrol-forecast-2025-2031>. [Accessed: 29-Apr-2025]
- [2] R. P. Patera, “Hazard Analysis for Uncontrolled Space Vehicle Reentry,” *Journal of Spacecraft and Rockets*, vol. 45, no. 5, pp. 1031–1041, Sep. 2008 [Online]. Available: <https://arc.aiaa.org/doi/10.2514/1.30173>. [Accessed: 23-Mar-2025]
- [3] E. Wright, A. Boley, and M. Byers, “Airspace closures due to reentering space objects,” *Sci Rep*, vol. 15, no. 1, p. 2966, Jan. 2025 [Online]. Available: <https://www.nature.com/articles/s41598-024-84001-2>. [Accessed: 06-Feb-2025]
- [4] Uber Technologies Inc., “H3: Uber’s hexagonal hierarchical spatial index.” [Online]. Available: <https://eng.uber.com/h3>
- [5] “Tables of Cell Statistics Across Resolutions | H3.” [Online]. Available: <https://h3geo.org/docs/core-library/restable>. [Accessed: 07-Feb-2025]
- [6] EUROCONTROL, “Aircraft Performance Database.” [Online]. Available: <https://contentzone.eurocontrol.int/aircraftperformance/>. [Accessed: 29-Jan-2025]
- [7] “SKYbrary Aviation Safety.” [Online]. Available: <https://skybrary.aero/>. [Accessed: 11-Apr-2025]
- [8] “Doc 8643.” [Online]. Available: <http://www.doc8643.com>. [Accessed: 11-Apr-2025]
- [9] S. Leiden, “SatTrackCam Leiden (b)log: Kosmos 482 Descent Craft reentry forecasts [UPDATED],” 24-Apr-2025. [Online]. Available: <https://sattrackcam.blogspot.com/2025/04/kosmos-842-descent-craft-reentry.html>. [Accessed: 29-Apr-2025]
- [10] J. C. McDowell, “General Catalog of Artificial Space Objects.” 2020 [Online]. Available: <https://planet4589.org/space/gcat>. [Accessed: 02-Mar-2025]
- [11] “The Space Review: Kosmos 482: Questions around a failed Venera lander from 1972 still orbiting Earth (but not for long).” [Online]. Available: <https://www.thespacereview.com/article/4384/1>. [Accessed: 30-Apr-2025]
- [12] J. J. Sellers *et al.*, *Understanding space: An introduction to astronautics*. McGraw-Hill Custom Pub., 2003 [Online]. Available: <https://books.google.be/books?id=IIcgAQAAIAAJ>



(a) Keplerian elements: semi-major axis,  $a$ , the distance between the foci,  $2c$ , the eccentricity,  $e = (2c)/(2a)$ . (the semiparameter (a.k.a. *semilatus rectum*),  $p$ , describes the size of the conic section by defining the width at the primary focus, and is defined as  $p = b^2/a = a(1 - e^2)$ )



(b) Keplerian elements: inclination,  $i$ , the right ascension of the ascending node,  $\Omega$ , and the argument of perigee,  $\omega$ . (Earth rotates around  $\hat{K}$ )

Figure 9: Definition of Keplerian elements. The orbital elements describing the trajectory of orbiting object are illustrated in association with an inertial reference frame  $\hat{I}\hat{J}\hat{K}$ . The  $I$ -axis,  $\hat{I}$ , points toward the vernal equinox and the  $J$ -axis,  $\hat{J}$ , is perpendicular to the  $I$ -axis in the equatorial plane n the sense of Earth's rotation with the  $K$ -axis pointing up. The semi-major axis,  $a$ , the eccentricity,  $e$ , the inclination,  $i$ , the right ascension of the ascending node,  $\Omega$ , and the argument of perigee,  $\omega$ , constitute, together with the mean anomaly at the initial position,  $M_0$ , a set of six constants of motion that are preserved in the absence of perturbation. True anomaly,  $\nu$ , specifies the location of an orbiting object within the orbit. It is the angle between perigee and the orbiting object's position vector measured in the direction of the orbiting object's motion. Figures from [12], respectively Figure 5-2 and Figure 5-9.